Journal of The Electrochemical Society, **156** (3) H220-H224 (2009)
0013-4651/2009/156(3)/H220/5/$23.00 © The Electrochemical Society

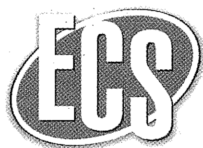

Optical Investigations of Directly Wafer-Bonded InP–GaAs Heterojunctions

Yan-Feng Lao,[z] Hui-Zhen Wu, Meng Cao, and Chun-Fang Cao

State Key Laboratory of Functional Materials for Informatics, Shanghai Institute of Microsystem and Information Technology, Chinese Academy of Sciences, Shanghai 200050, China

The optical characteristics of directly wafer-bonded InP–GaAs heterojunctions have been investigated. By designing the bonding interface at standing-wave antinode, its influence on optical performances of bonded structures is magnified, which facilitates experimental detection using optical methods. Wavelength blueshift and reflectivity falling at the resonance mode were observed in wafer-bonded InP–GaAs heterostructures. Numerical analysis suggests that two effects involving thickness change of interfacial bonding layers and extra optical loss introduced by bonded junctions are responsible for the experimental observations, and these effects can be attenuated by lowering anneal temperatures and incorporating an InP/InGaAsP superlattice into the surface of InP-based materials. The results are useful for designing effective optical characteristics of wafer-bonded device structures.
© 2009 The Electrochemical Society. [DOI: 10.1149/1.3071521] All rights reserved.

Manuscript submitted October 14, 2008; revised manuscript received December 18, 2008. Published January 29, 2009.

Direct wafer bonding has become an important technique for integrating lattice-mismatched materials. A wide range of material systems, such as GaAs/InP,[1] InP/Si,[2] GaAs/Si,[3] GaAs/GaN,[4] GaN/GaN,[5] ZnO/GaN,[6] etc., has been successfully integrated by using this technique and various wafer-bonded devices such as vertical-cavity surface-emitting lasers (VCSELs),[7] light-emitting diodes,[8] detectors,[9] vertical couplers,[10] avalanche photodiodes,[11] AlGaAs/GaAs/GaN heterojunction bipolar transistors,[12] etc., have been demonstrated with optimum performances as compared to their corresponding counterparts based on conventional epitaxial-based integration methods.

However, the influences of the wafer-bonding process on electrical and optical characteristics should be first investigated for its successful application in optoelectronic devices. Multiple references[13-15] have systematically studied the electrical properties and provided optimizing conditions for wafer bonding. Actually, the conduction problem can be avoided by using intracavity electrodes bypassing the bonded junctions.[7] On the contrary, the propagation of light inside semiconductors and thus inevitable absorbing and scattering at the bonded heterointerface have an effect on the optical performances of wafer-boned structures. Minimizing optical loss by placing the bonding interface at an optical-field minimum is the basic design rule for vertical-cavity devices, such as VCSELs.[16] High-performance long-wavelength (1.3–1.6 μm) VCSELs based on the wafer-bonding heterointegration technique illustrate the fact that little optical loss is introduced by the bonding process. However, a better understanding to optical characteristics is of vital importance for further wafer-bonded device optimization and commercial application. Direct studies are still absent. Liu et al.[9] have compared the optical propagation loss of the wafer-bonded waveguide with the unbonded one and evaluated the net optical loss of the bonded junction. But light in the waveguide travels in parallel with the bonding interface, which is different from the situation of light propagating vertical to the interface in vertical-cavity devices.

In this paper, we present a method to investigate the optical properties of directly wafer-bonded heterojunctions. InP–GaAs bonded structures were designed to be Fabry–Pérot (F-P) resonators in which the bonding interface is placed at standing-wave antinode to increase overlapping of optical field and the bonded junction. This design magnifies the influence of the InP–GaAs heterojunction on its optical performances and facilitates optical detection. Wavelength blueshift and reflectivity falling at the resonance mode were observed in InP–GaAs bonded structures. Two effects involving the thickness change of interfacial bonding layers and extra optical loss introduced by bonded junctions are then proposed and discussed by numerical simulation based on the transfer-matrix method (TMM).

[z] E-mail: lyflys@hotmail.com

Experimental

Both InP and GaAs-based materials (Fig. 1) were grown by gas-source molecular-beam epitaxy. Before bonding, wafers were cleaved into 1 × 1 cm squares. The surfaces of InP-based samples were patterned with a channel of 250 × 300 μm by chemical etching. They were first cleaned in analytical reagent sulfuric acid (H_2SO_4) and aqueous-based $3H_2SO_4 + 1H_2O_2 + 1H_2O$ solutions for <10 s to remove possible organic contamination during photolithography process. To remove surface oxide, wafers were dipped into aqueous-based hydrogen fluoride solutions ($1HF + 10H_2O$). Then they were transferred into methanol solutions and joined face to face with ⟨011⟩ direction aligned. The pressure was applied by a steel fixture that was annealed in the nitrogen (N_2) ambient. Load pressure and annealing time were fixed to 3 MPa and 30 min, respectively, for all wafer-bonded samples.

After bonding, InP and InGaAsP materials were selectively etched by $3HCl + 1H_2O$ and $1H_2SO_4 + 1H_2O_2 + 10H_2O$ solutions, respectively. The reflection spectra were measured by a NICOLET 860 Fourier transform IR spectroscopy.

Results and Discussion

Optical properties of designed structures.— The single-pass optical-loss of a layer in an F-P resonator is calculated by

$$\text{loss} = 1 - \exp(-\bar{\alpha}L_{\text{eff}}) \approx \bar{\alpha}L_{\text{eff}} \quad [1]$$

where L_{eff} is the effective cavity length and

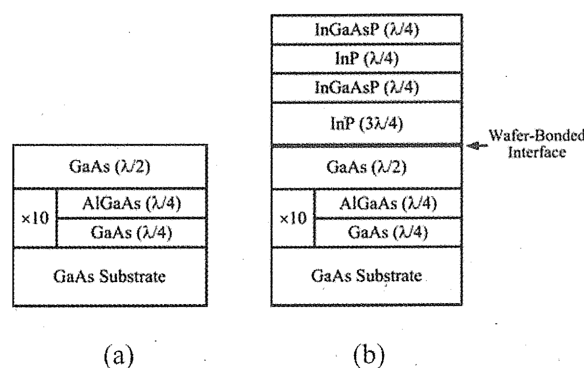

Figure 1. Schematic diagram of (a) the GaAs/AlGaAs periodical structure and (b) the InP–GaAs wafer-bonded structure.

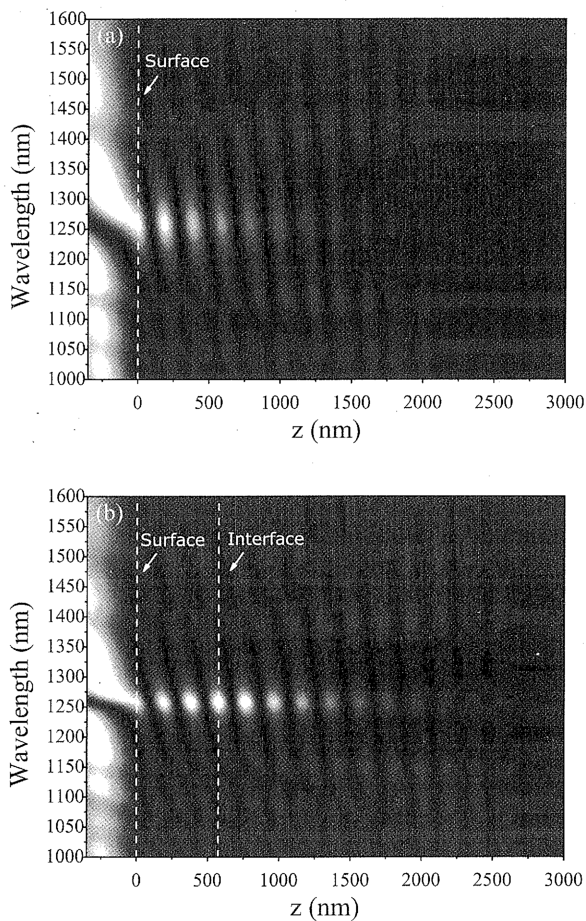

Figure 2. Calculated optical field of (a) the GaAs/AlGaAs structure and (b) the InP–GaAs wafer-bonded structure.

$$\bar{\alpha} = \left(\frac{\xi d}{L_{\text{eff}}}\right)\alpha \qquad [2]$$

in which ξ, d, and α are the standing-wave enhancement factor, thickness, and absorption coefficient of the layer, respectively. $\xi d/L_{\text{eff}}$ represents the optical confinement factor.[17] Thus

$$\text{loss} = \xi d\alpha \qquad [3]$$

By placing the layer at the standing-wave antinode, the enhancement factor ξ and, thus, optical loss are maximized.

To facilitate optical investigation of the bonded junction, we designed the InP–GaAs integrated structure to be an F-P resonator as shown in Fig. 1b. Numerical calculation indicates that the GaAs/$Al_{0.93}$GaAs periodical structure (Fig. 1a) forms an F-P resonator as well in which the semiconductor/air index step acts as the top mirror. Denotations, such as $3\lambda/4$, $\lambda/2$, etc., in Fig. 1, represent the optical thickness of the corresponding layer. The resonance characteristics of both structures are verified by calculating their optical field distribution as shown in Fig. 2a and b. The brightness represents the region with greater optical intensity. It can be seen that the surface of GaAs/AlGaAs periodical structures (Fig. 1a) and the InP–GaAs heterointerface of wafer-bonded structures (Fig. 1b) both lie at the standing-wave antinode. This design maximizes the overlapping of optical field and the bonded junction. When extra optical loss, including light absorbing and scattering, appears in the bonded junction, our designed structures magnify these two effects and lead to a maximum falling of reflectivity. Therefore, the structure of Fig. 1b is designed at a maximal extent for optically investigating the wafer-bonded junction.

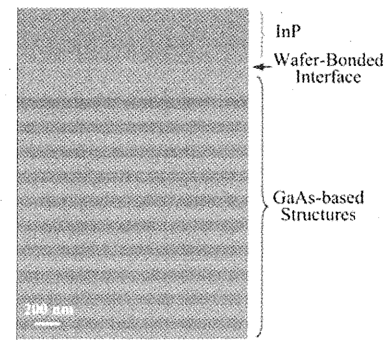

Figure 3. Cross-sectional SEM of the InP–GaAs bonded sample.

In the experiment, we study the optical properties of wafer-bonded structures by measuring their reflection spectra. The GaAs/AlGaAs periodical structure composes the distributed Bragg reflector (DBR) of VCSELs. The position of its high reflectivity affects the lasing mode of the whole VCSEL structure. In the following parts, we first investigate the variation of optical performances of GaAs-based structures (Fig. 1a) on different processing conditions, then numerically analyze the influence of bonded junctions by simulating the reflection spectra of InP–GaAs wafer-bonded structures in the theoretical scheme of TMM.

Optical characterization of GaAs-based materials.— A set of GaAs-based samples with the structure of Fig. 1a are prepared under different conditions. Two bonding-processed GaAs-based samples were obtained by first bonding the InP–GaAs structures at 580 and 630°C, respectively, and then selectively chemical removing InP-based materials. A cross-sectional scanning electron microscope (SEM) image in Fig. 3 shows that the InP–GaAs bonding interface is uninterrupted and well bonded. The other two samples were annealed at the same temperature of 580°C with and without a proximity cap of an InP substrate, respectively. Figure 4 illustrates their refection spectra. The resonance wavelength (λ_C) of all processed samples is blueshifted as compared to that of the as-grown structure. It can be seen that higher anneal temperatures and the wafer-bonding process result in much more blueshift of λ_C.

Generally, two changes are triggered during the annealing process: element interdiffusion inside the structure and material decomposition at the surface. For GaAs/AlGaAs periodical structures, Al–Ga interdiffusion takes place at high temperatures, which modifies the refractive index profile and blueshifts the λ_C. We will then discuss the contribution of this effect to the shift of λ_C in the next section. For samples annealed at the same temperature, however, surface material modification is the main reason for the blueshifted λ_C. At 580°C, GaAs decomposition due to arsenic escaping and Ga atoms diffusing decreases the thickness of surface $\lambda/2$ layer in Fig. 1a to some degree and, thus, blueshift the λ_C. Greater blueshift of λ_C was observed in the sample annealed without a proximity cap, indicating that serious surface material loss takes place in this sample, whereas, little change of λ_C was observed in the sample annealed with a proximity cap. The capped InP substrate acts as a barrier preventing continuous decomposition of surface materials.[18] As we can see from Fig. 4, the blueshift of λ_C in the wafer-bonded sample is more than that in the proximity-capping annealed sample, the pressure applied during the bonding process plays an important role in this different shift of λ_C. Under high-temperature annealing, gaseous group-V and liquid group-III elements coexist at the interface. The applied pressure might squeeze these substances out of the interface and evens out the surface. In addition, pressure induces the transformation of interfacial crystallography.[19] An amorphous layer has been observed at the bonding interface.[20,21] These variations contribute to the optical-thickness change of interfacial bonding layers and the shift of λ_C.

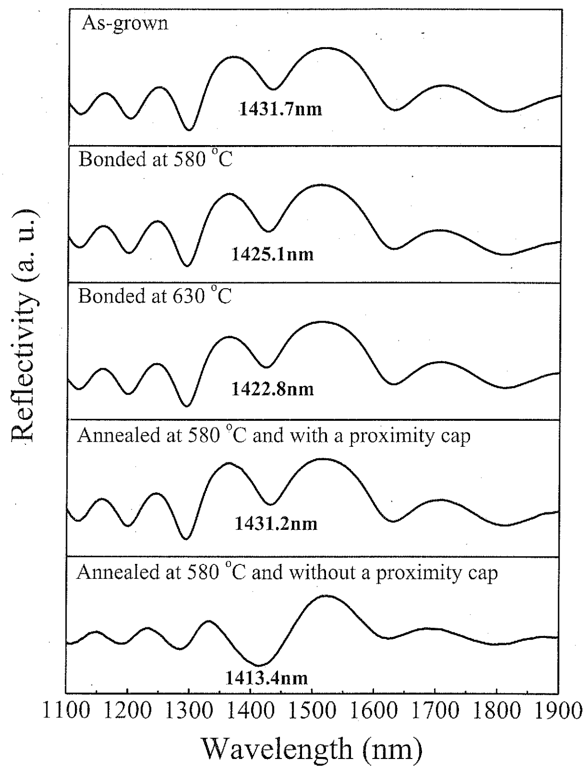

Figure 4. Reflection spectra of the GaAs/AlGaAs periodical structures under different processing conditions.

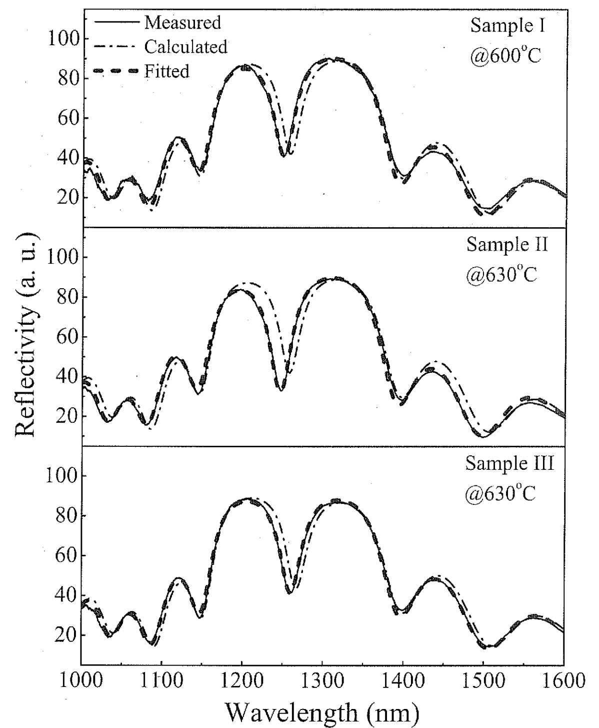

Figure 5. Comparison of measured, calculated, and fitted reflection spectra of samples I–III, respectively.

From Fig. 4, the blueshift of λ_C for the 580°C-bonded samples is 6.6 nm compared to that of the as-grown structure, and that increases to 8.9 nm when the anneal temperature is at 630°C. This blueshift value is relatively small in comparison to the width of high-reflectivity band of GaAs/AlGaAs DBRs and thus has little effect on the shift of lasing mode.

Numerical analysis of wafer-bonded InP–GaAs heterojunctions.— For the wafer-bonded device, its structure involves a heterojunction. As a result, bonding effects include the variations from both InP and GaAs side materials beside the heterointerface. Quantitatively evaluating structure variations contributing to the blueshift of λ_C and extra optical loss of the bonded junction is useful for designing the optical characteristics of wafer-bonded InP–GaAs devices. In this investigation, three InP–GaAs bonded samples (named I, II, and III) were fabricated by using two kinds of InP-based structures with different $3\lambda/4$ layers. Samples I and II have the same $3\lambda/4$ layer, consisting of InP, and were bonded at 600 and 630°C, respectively. Sample III was bonded at 630°C, but the $3\lambda/4$ layer is composed of a five-period 6.9 nm–InP/8.7 nm–InGaAsP superlattice (SL). The GaAs/AlGaAs periodical structure with different λ_C from that of the sample in the previous section was used for samples I–III. After bonding, selective chemical etching was applied to obtain the structure of Fig. 1b. Figure 5 shows their reflection spectra. The calculated curves using as-grown parameters were drawn as well. To ensure numerical accuracy, structural parameters were first measured by high-resolution X-ray diffraction and then finely adjusted so that calculated curves are well matched with measured reflection spectra of as-grown samples. Wavelength-dispersion relation of the refractive index was considered during calculation. We can see from Fig. 5 that λ_C of wafer-bonded samples is blueshifted and the reflectivity at λ_C is decreased, which indicates that structural transformation appears in bonding structures.

We first numerically analyze the variation of optical performances of GaAs-side materials and fit the parameters describing wafer-bonding effects. Then these parameters are used to simulate the reflection spectra of InP–GaAs bonded structures to achieve parameters for the InP-side materials. For instance, sample II is selectively etched to obtain the GaAs-based material with the same structure of the as-grown one (Fig. 1a). Figure 6a shows the comparison of reflection spectra of the bonding-processed GaAs-based sample with those of the as-grown structure. Two variations involving element interdiffusion and material decomposition are used to explain the shift of λ_C. We first consider the effect of Al–Ga interdiffusion as the redistribution of Al composition satisfying Fick's equation[22]

$$x_{Al}(z,t) = x_{Al}(z,\infty) + \frac{2}{\pi}(x_l - x_h) \times \sum_n \frac{1}{n}\cos(n\pi)\sin\left(\frac{n\pi d_l}{T}\right)\cos\left(\frac{2n\pi z}{T}\right) \times \exp\left[-\left(\frac{2\pi}{T}\right)^2 nL_D^2\right] \quad [4]$$

$$x_{Al}(z,\infty) = \frac{d_h x_h + d_h x_h}{T} \quad [5]$$

$$T = d_l + d_h \quad [6]$$

where $x_{Al}(z,t)$ is the Al composition at position z and time t. $x_{Al}(z,\infty)$ represents average Al composition after infinite time of interdiffusion. x_l, d_l and x_h, d_h are the composition and thickness of lower Al-composition layer and higher Al-composition layer, respectively. L_D is the diffusion length

$$L_D = \sqrt{D_{Al\text{-}Ga}t} \quad [7]$$

in which $D_{Al\text{-}Ga}$ is the interdiffusion coefficient and t is the annealing time. By assuming that $D_{Al\text{-}Ga}$ equal to 1×10^{-16} and 5×10^{-16} cm^2/s, the refractive index profile of the GaAs/AlGaAs periodical structure is modified as shown in Fig. 6b, which results in the change of reflection spectra (Fig. 6c) with different blueshifted λ_C. But the λ_C under these two $D_{Al\text{-}Ga}$ is still longer than the mea-

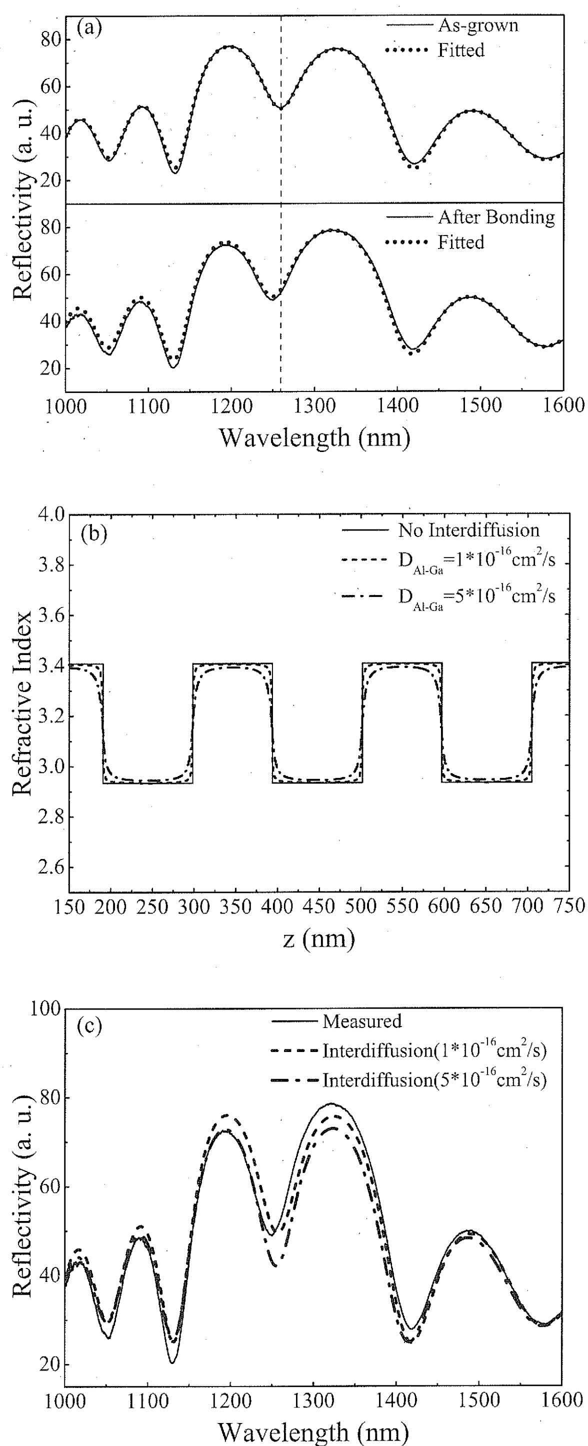

Figure 6. (a) Comparison of measured and fitted reflection spectra of GaAs-based materials obtained by chemical removing the InP-based materials of sample II, (b) refractive index profile with different Al–Ga interdiffusion coefficients, and (c) comparison of measured and calculated reflection spectra using the refractive index profile of (b).

sured value, indicating that much greater D_{Al-Ga} should be assumed in the calculation. In fact, a high-temperature annealing process up to 850°C is needed to obtain the interdiffusion coefficient of 5 $\times$ 10^{-16} cm^2/s,[23] but the anneal temperature of sample II is only 630°C. Therefore, Al–Ga element interdiffusion cannot account for the blueshift of λ_C.

As analyzed in the previous section, material loss could exist at the bonding interface of wafer-bonded samples. To simulate the reflection spectra of Fig. 6a, we propose that the optical thickness of interfacial layers close to the bonding interface is reduced (δL represents the value of variation). By setting δL(GaAs) equal to 15.4 nm, the measured spectrum is well fitted as shown in Fig. 6a. At this point, the blueshift of λ_C can be ascribed to optical-thickness decrease of interfacial bonding layers. This result indicates that the blueshifted λ_C can be compensated by increasing cavity thickness.

Table I. Numerical results of the Inp–GaAS wafer-bonded structures.

Sample	Blueshift of λ_C (nm)	$\delta L/\alpha$ in InP side (nm/cm^{-1})	$\delta L/\alpha$ in GaAs side (nm/cm^{-1})	Single-pass optical loss (%)
I	8.3	16.1/500	12.0/300	0.010
II	11.2	24.1/5400	15.4/1400	0.086
III	6.7	11.3/700	15.4/1400	0.028

It can be seen from Fig. 6a that the measured reflectivity (R_C) at λ_C is slightly less than the calculated value. Because the reflection spectrum of the as-grown sample is well fitted, this phenomenon does not result from numerical calculation. Microstructure transformation in the heterointerfacial region on the wafer-bonding process has been observed.[14,15,20,21] Interfacial defects, such as dislocations, voids, cavities, etc., are verified by micro-observations such as transmission electron microscopy. Recombination centers close to the interface were identified by electron-beam-induced current[24] and cathodluminesoence[25] measurements. Jin-Phillipp et al.[21] found that elements interdiffuse at the InP–GaAs bonding interface causing a 6–8 nm interfacial region. The cavities composed of amorphous and crystalline mixed structures were verified in their observation with a dimension of 6–8 nm as well. Moreover, secondary ion mass spectroscopy measurements[15] revealed the distribution of oxygen at bonding interface with an exponentially decayed lateral range of tens of nanometers. On the basis of this evidence, we ascribe the falling of R_C in our wafer-bonded samples to the extra optical loss introduced by the bonded junctions. In the simulation, we assume the interfacial layer close to the bonding interface has a uniform absorption coefficient (α) and its thickness is 20 nm, which is the upper limit of observed dimension of interfacial cavities and elements diffusion.[15,21] By setting α(GaAs) equal to 1400 cm^{-1}, the measured R_C is well fitted. In a similar way, parameters of δL and α for the GaAs side materials in samples I and III are fitted as well and listed in Table I. These parameters are then used to simulate the measured reflection spectra of samples I–III to fit the parameters of InP side materials. Figure 5 shows that the fitted spectra are well matched to the measured curves. Numerical results are summarized in Table I. Because wafer bonding is a thermal process, transformations of interfacial microstructures are induced by high-temperature annealing. Lowering anneal temperatures thus attenuate the wafer-bonding effects. In addition, the InP/InGaAsP SL has been proven to act as a defect-blocking layer, preventing the propagation of dislocations.[26] In our experiment, similar results were observed. The incorporation of an InP/InGaAsP SL greatly decreases the blueshift of λ_C and optical loss even at a higher bonding temperature up to 630°C.

Considering the practical configuration of devices with the wafer-bonded junction placed at the standing-wave node, the total single-pass optical losses calculated by using the formula $\xi_{InP}\alpha_{InP}d_{InP} + \xi_{GaAs}\alpha_{GaAs}d_{GaAs}$ are 0.0103, 0.0860, and 0.0280%, corresponding to samples I, II, and III, respectively, which are of comparable value to other optical losses, such as tunnel junction, aperture scattering, etc.[27]

Conclusions

The optical characteristics of directly wafer-bonded InP–GaAs heterojunctions were investigated by using an F-P resonator structure in which the bonding interface was placed at a standing-wave

antinode to magnify bonding effects and facilitate optical detection. After bonding, wavelength blueshift and reflectivity falling were observed in the wafer-bonded structures. Analysis suggests that interfacial microstructure transformations involving thickness change of interfacial bonding layers and extra optical loss introduced by bonded junctions are responsible for these experimental observations. Numerical results show that the extra optical loss is comparable to other loss sources, such as tunnel junction, aperture scattering, etc., and can be decreased by incorporating an InP/InGaAsP SL into the surface of InP-based materials and lowering anneal temperatures. Results are useful for designing effective optical characteristics of wafer-bonded device structures.

Acknowledgment

This work was supported by the State Key Development Program for Basic Research of China under grant no. 2003CB314903.

Chinese Academy of Sciences assisted in meeting the publication costs of this article.

References

1. Z. L. Liau and D. E. Mull, *Appl. Phys. Lett.*, **56**, 737 (1990).
2. K. Mori, K. Tokutome, K. Nishi, and S. Sugou, *Electron. Lett.*, **30**, 1008 (1994).
3. Y. H. Lo, R. Bhat, D. M. Hwang, C. Chua, and C.-H. Lin, *Appl. Phys. Lett.*, **62**, 1038 (1993).
4. J. Jasinski, Z. Liliental-Weber, S. Estrada, and E. Hu, *Appl. Phys. Lett.*, **81**, 3152 (2002).
5. T. Tokuda and S. Noda, *Jpn. J. Appl. Phys., Part 2*, **39**, L572 (2000).
6. A. Murai, D. B. Thompson, C. Y. Chen, U. K. Mishra, S. Nakamura, and S. P. Denbaars, *Jpn. J. Appl. Phys., Part 2*, **39**, L1045 (2006).
7. V. Jayaraman, M. Mehta, A. W. Jackson, S. Wu, Y. Okuno, J. Piprek, and J. E. Bowers, *IEEE Photonics Technol. Lett.*, **15**, 1495 (2003).
8. Y. H. Lo, R. Bhat, D. M. Hwang, M. A. Koza, and T. P. Lee, *Appl. Phys. Lett.*, **58**, 1961 (1991).
9. B. Liu, A. Shakouri, P. Abraham, B. G. Kim, A. W. Jackson, and J. E. Bowers, *Appl. Phys. Lett.*, **72**, 2637 (1998).
10. Y. Kang, P. Mages, A. R. Clawson, S. S. Lau, Y. H. Lo, P. K. L. Yu, A. Pauchard, Z. Zhu, and Y. Zhou, *Appl. Phys. Lett.*, **79**, 970 (2001).
11. A. R. Hawkins, T. E. Reynolds, D. R. England, D. I. Babic, M. J. Mondry, K. Dtreubel, and J. E. Bowers, *Appl. Phys. Lett.*, **68**, 3692 (1996).
12. C. Lian, H. (Grace) Xing, C. S. Wang, L. McCarthy, and D. Brown, *IEEE Electron Device Lett.*, **28**, 8 (2007).
13. H. W. Y. Ogawa and T. Kamijoh, *Appl. Phys. Lett.*, **62**, 738 (1993).
14. F. Shi, K. L. Chang, J. Epple, C. F. Xu, K. Y. Cheng, and K. C. Hsieh, *J. Appl. Phys.*, **92**, 7544 (2002).
15. F. Salomonsson, K. Streubel, J. Bentell, M. Hammar, D. Keiper, R. Westphalen, J. Piprek, L. Sagalowicz, A. Rudra, and J. Behrend, *J. Appl. Phys.*, **83**, 768 (1998).
16. D. I. Babic, J. Piprek, K. Streubel, R. P. Mirin, N. M. Margalit, D. E. Mars, J. E. Bowers, and E. L. Hu, *IEEE J. Quantum Electron.*, **33**, 1369 (1997).
17. S. W. Corzine, R. S. Geels, J. W. Scott, R. H. Yan, and L. A. Coldren, *IEEE J. Quantum Electron.*, **25**, 1513 (1989).
18. J. A. del Alamo and T. Mizutani, *J. Appl. Phys.*, **62**, 3456 (1987).
19. K. L. Chang, G. WPickrell, K. Y. Cheng, and K. C. Hsieh, *Semicond. Sci. Technol.*, **19**, 906 (2004).
20. L. Sagalowicz, A. Rudra, E. Kapon, M. Hammar, F. Salomonsson, A. Black, P.-H. Jouneau, and T. Wipijewski, *J. Appl. Phys.*, **87**, 4135 (2000).
21. N. Y. Jin-Phillipp, W. Sigle, A. Black, D. Babic, J. E. Bowers, E. L. Hu, and M. Ruhle, *J. Appl. Phys.*, **89**, 1017 (2001).
22. P. D. Floyd and J. L. Merz, *J. Appl. Phys.*, **76**, 5524 (1994).
23. J. D. Ralston, S. OBrien, G. W. Wicks, and L. F. Eastman, *Appl. Phys. Lett.*, **52**, 1511 (1988).
24. R. J. Ram, J. J. Dudley, J. E. Bowers, L. Yang, K. Carey, S. J. Rosner, and K. Nauka, *J. Appl. Phys.*, **78**, 4227 (1995).
25. Y. Ohiso and C. Amano, *J. Appl. Phys.*, **87**, 2857 (2000).
26. K. A. Black, P. Abraham, A. Karim, J. E. Bowers, and E. L. Hu, 11th International Conference on Indium Phosphide and Related Materials, May 16–20, 357 (1999).
27. D. Feezell, D. A. Buell, D. Lofgreen, M. Mehta, and L. A. Coldren, *IEEE J. Quantum Electron.*, **42**, 494 (2006).